Internal Report
DESY-F15-83-01
August 1983

ARGUS MAGNETIC FIELD MEASUREMENTS

by

R.L. Childers

University of South Carolina, USA

Y. Oku

University of Lund, Sweden

ABSTRACT

This report describes the measurement and parametrization of the ARGUS magnetic field. The field calculated from the parameters reproduces the measured field to within a few parts per thousand.

CONTENTS

I. Introduction
II. Apparatus, Calibration and Measurements
III. Magnetization
IV. Stray Fields
V. Symmetry
VI. Tangential Components B_φ
VII. Axial and Radial Component B_z and B_ρ
VIII. Parametrization
IX. Other Regions
X. Acknowledgements

I. Introduction

The magnetic field intensity in the interior of the ARGUS detector was measured between 27 March and 2 April, 1982. The volume in which most of the measurements were made was essentially that to be occupied by the drift chamber (Figure 1). The BEBC-field mapping system from CERN was used to make and record the measurements.

Measurements were made of the field components B_z, B_ρ and to a lesser extent, B_φ, for three different configurations of the inner compensation coils. Figure 2 shows the coordinate system used. The compensation coil configurations, or connection schemes, are designated 100%, 50%, and 0% compensation and are shown in Figure 3. The discovery of a high-resistance short-to-ground in coil number four on the +z side dictated the use of the coil configurations shown because it was not possible to repair the coil in less than several months. The measurements made and the spacing between the measured points was to some extent dictated by the time available.

The data were recorded on duplicate floppy discs from which IBM tapes were later prepared at CERN and sent to DESY. The B_z and B_ρ components have been parameterized and an analytic expression found for the B_φ component.

Prior to the main field measurements a series of measurements was made to determine the effect of the magnet's immediate history on the field. The stray field also was measured at a number of places outside the main magnet coil. Other runs were made to check the reproducibility of the probes and the reproducibility of the mechanical positioning mechanism. All measurements, with the exception of the magnetization measurements, were made at 95% of the maximum rated current of the power supply (4275 amps). With the current flowing in the normal direction the solenoid corresponds to a bar magnet with its north pole at the east (+z) end of the ARGUS detector. (B_z is negative).

II. Apparatus, Calibration and Measurement

When the magnet is energized the only access to the field region is through the central axis of the mini-beta quadrupoles. (Fig. 1). The mechanical positioning of the probes, as well as the feed-through for the cables, had to be made through these holes. A sketch of the mechanical framework for holding and moving the probes is shown in Fig. 4. The supports I, II and III on which the hall probes were mounted were fixed with respect to one another and could be moved along the z axis as a unit by means of the hollow tube 1. The cables for the 185 hall probes passed through this tube. The tube 1 was attached to a carriage which could be remotely positioned with a precision of 0.2 mm along the z axis. The spacing between the measuring points was 50 mm in the z and ρ direction and 30^{0} in φ (Figure 5).

The measuring procedure was to start with the apparatus at some fixed angle and at the east end of the magnet. All of the probes were then read out. The carriage was then advanced 50 mm and the probes read out again. This continued automatically until the western limit had been reached. Then the apparatus was returned to the eastern end and rotated to a new angle and the procedure repeated. As a check one complete traverse along the z axis was repeated. In addition to the hall voltages, the temperature in the magnet, the magnet current and the time were recorded on the floppy disks.

The probes in their mounts were calibrated at CERN against an NMR probe using a magnet of uniform field. They were calibrated as a function of temperature and of magnetic field. A separate calibration curve was established for each probe. When the differences between the NMR values and those determined from the calibration constants is plotted, the width at half-maximum of the distribution is approximately 5 Gauss.

III. Magnetization

A series of measurements was made to detect the effect of the magnetic history of the iron yoke on the magnetic field for a given excitation current. This was done by varying the current while keeping the probes fixed at one position. The readings of one probe as a function of current are shown in

Fig. 6. To a good approximation there was no observed effect due to the history, and the data fit a straight line with a r.m.s. deviation of 7 Gauss.

During these measurements it was found that the power supplies could not continuously deliver the maximum rated current. For this reason it was decided to make all readings at 4275 A, which is 95% of the maximum rated current. This is the current used during data taking.

IV. Stray Fields

The stray fields outside the coil were measured at some of the photomultiplier tube housing positions. After the main magnetic field measurements were made, the current was set to zero and the stray fields measured. The zero current fields were nowhere greater than five Gauss, typical values being less than two Gauss. With the magnet and compensation coils excited, typical values for B_z were less than 35 Gauss, those for B_ρ less than 15 Gauss. With the exception of the regions near the current connections for the main coil the field was nowhere greater than 70 Gauss.

V. Symmetry

Two types of geometrical symmetry were checked for : symmetry in φ and symmetry in z. Only the B_z component was considered because the B_ρ data required too many corrections to be usefully employed for this purpose.

If the field is symmetric in φ a given probe should read the same at all angles. A histogram of the difference between the average for all angles and the value at one angle reflects any deviation from symmetry. If there is no asymmetry the histogram will reflect the reproducibility of the probes and precision of mechanical alignment. The first two columns in table I show the r.m.s. values of this distribution for each compensation, first in percent and then in Gauss.

A similar test was made of the symmetry about the midplane (z=0) by subtracting the readings at each value of +z from the value at the corresponding point at -z. The r.m.s. values of this distribution are shown in the third and fourth columns of Table I.

To determine the relative importance of the asymmetries, they have been compared with an estimate of the measurement uncertainty. Due to the overlap region between the supports it is possible to read the field at the same point in space with two different probes. The r.m.s. average of the differences between two probes reading the same point has been taken as an estimate of the measurement error. This way of estimating the measurement error will include the effects of probe misalignment. These are listed in columns five and six of Table I. The increase in measurement error with greater compensation reflects the fact that precision in position is more important in non-uniform fields. That the errors are larger for the radial component than for the axial component is expected from the discussion later in Axial and Radial Components.

A comparison of the values in Table I lead to the conclusion that the field is symmetric within the measurement errors, both in φ and about the plane $z = 0$.

VI: The Tangential Component (B_φ)

One does not expect a φ component for the magnetic field of a perfect solenoid. A number of things can give rise to such a component for real solenoids; for instance, the coil may not be perfectly circular, or there are unaccounted- for currents. There is not, however, a contribution inside the coil due to the longitudinal component of the current in the coil. This gives rise to a field outside the coil which is the same as that due to a straight wire on the axis and carrying the same current as the coil. In order to detect any φ component seven probes were placed so as to measure B_φ. They were placed at the ends of the long arms on supports I and III. (See Fig. 4). The observed field readings were not zero and ranged from -100 Gauss to +200 Gauss.

The observed values of B_φ seem to be satisfactorily explained by the sum of several terms;

B_α : When a probe is not perfectly aligned it will detect less of the component for which it is intended and will detect some part of the other components. Since B_z is large, the misalignment of a probe by only 5 milliradians can change the probe's reading by 35 Gauss. B_α is a term due to the gross misalignment of a probe with respect to the coordinate system of the measuring machine.

B_{k_1} : If the axis of rotation of the measuring machine is not parallel to the symmetry axis of the field, there will be a change in the B_φ projection of the B_z component as the machine is rotated about its axis. This can not easily be shown in a static drawing, but can easily be seen by making a simple cardboard model and rotating it. This term can be approximated by $k_1 (90-\varphi)$ if the machine axis is in the y-z plane but not parallel to the z axis. The constant k_1 should be the same for all probes.

B_{k_2} : If there is some rocking of the axis as the machine is rotated, due, for instance, to imperfections in the bearing rings at the end, another variation is introduced. If the motion of this axis is entirely in the y-z plane, the contribution to the probe reading can be approximated by $k_2 |90-\varphi|$ where $0 < \varphi < 180$. The restriction on the angle corresponds to the way in which measurements were actually made. The constant k_2 should also be the same for all probes.

B_{wire} : The coils are separated by a spacing of 5 cm. (See Figure 1), and are connected to the adjacent coil at the same angular position by conductors which are 165 cm from the z-axis. If one assumes that far from the connector they can be treated as a long straight wire, and if one takes into account the orientation of the hall probes and the direction of the magnetic field, then an analytic expression for this term can be written.

If the above four terms are the only ones, then one can write

$$B_\alpha(\text{observed}) = B_\alpha + k_1\,(90-\varphi) + k_2\,|(90-\varphi')| + 885\,\frac{\rho - 165\cos(180-\varphi)}{\rho^2+(165)^2-330\cos(180-\varphi)} \qquad (1)$$

where ρ is the distance from the z axis to the probe in question. The geometry of the placement of the probes on the different supports requires that for support III $\varphi' = \varphi$ and for support I $\varphi' = \varphi - 180^o$. The same considerations require $k_2' = k_2$ for support III and $k_2' = -k_2$ for support I.

B_α is different for each of the seven probes but may easily be determined from the $\varphi = 90^o$ reading. The constants k_1 and k_2 should be approximately the same for each probe if the above argument is correct in its essentials. The reading of each probe as a function of φ was fit by a least-squares technique to the above equation. The parameters were found to be quite closely grouped. When all the probes are fit at once with the above two-parameter equation, B_α having been determined from the previous fit, the parameters are $k_1 = -0.11$ and $k_2 = 0.04$. The residuals between the prediction of the equation with the above parameters and the measured values are shown in Figure 7. The r.m.s. value of the distribution is 1.4 Gauss.

The closeness of the fit strongly suggests that the only real B_φ component is that due to the connectors between the coils. This does not need to be parametrized and in the volume occupied by the drift chamber is given by the expression for the field due to a long wire carrying 4275 A located 165 cm from the z axis at $\varphi = 180^o$.

Credence is given to this view by looking at a plot of B_φ vs. z for several probes in Figure 8. Note that the period of the fluctuation of the probes corresponds to the coil-to-coil spacing and that as one goes away from the coil connectors the curve becomes smoother.

VII. Axial and Radial Components; B_z and B_ρ:

For each of the three compensation coil configurations the components B_z and B_ρ were each measured at 7224 points (43 points along the z-axis x 14 radial positions x 12 angles, see Fig. 5). The space between the measuring points in the z-ρ plane was 5 cm and readings were taken every 30^o. The innermost probe was 20 cm from the z axis and the outermost was 85 cm.

The two principle sources of error for most of the measuring volume were probe calibration error and probe alignment error. The calibration errors are within allowable limits but the geometrical alignment and positioning errors were corrected for in some cases.

If a probe is intended to read a field B_n, to which it is nominally perpendicular, but is in fact misaligned by some small angle α, the reading will be

$$B_{obs} = \cos\ B_n \pm \sin\alpha\ B_p \qquad (2)$$

when B_p is the field component perpendicular to the intended field component.

For the B_z component $B_n \approx 8{,}000$ Gauss and B_p (the ρ component) is of the order of 400 Gauss at most. This means that an 8,000 Gauss field would, for a misalignment of .0175 radians (1^o) be read as 8 Gauss less than 8000 Gauss, or 1 part in 10^{+3} too small. Since the construction of the apparatus gives the best angular positioning to the probes which measure B_z (estimated to be $\pm$ 5 m rad) the B_z readings have been taken without any corrections. The differences between the probe readings in the overlap region is typically less than $1/10^3$ and no adjustment has been made. Figures 9, 10 and 11 display the measured B_z field without any corrections. The field is essentially the same at all angular slices through the chamber volume. (See section V, on symmetry).

When the raw B_ρ data were plotted they were found to be quite unsymmetric about the $z = 0$ plane. This would not be expected to be the case because a relatively high degree of symmetry was observed in the z component. If the field is exactly symmetric about the mid plane and has no φ compo- nent, then $B_\rho = 0$ at $Z = 0$. However, this lack of observed symmetry is easi- ly understood because the roles of the components are interchanged in Equation 2. If a probe is slightly misaligned by some angle α, each reading will have an additional component of $\sin\alpha B_z$, which will be 40 Gauss for a 5 mrad misalignment in an 8000 Gauss B_z field. To correct for this, an amount $\Delta_1 B_\rho$ was added to, or subtracted from the reading of each B_ρ probe on support II to make it read zero at the $z = 0$ plane. Using the measured value of B_z for the same location, an angular misalignment was found for each probe on support II ($\sin\alpha = \frac{\Delta_1 B_\rho}{B_z(z=0)}$). The readings of each probe on support II were then corrected for each position of z by adding (or subtracting) the quantity $\sin\alpha \cdot B_z(z,\rho)$. This process was continued at the overlap regions, finding an angular misalignment for the probes on plates I and II and cor- recting their readings by $\sin$ $B_z(z,\rho)$, where again $B_z(z,\rho)$ is the measured value of B_z at that point. Figures 12, 13 and 14 show the shape of the B_ρ component of the fields, corrected as indicated above. Note that although the field is relatively uniform over most of its volume, it is increasingly inhomogenious near the compensation coils as the percentage compensation increases.

VIII. Parametrization

It is useful to employ a coordinate system which displays the same symmetry as the field being parametrized. In the case of cylindrical symmetry the most obvious choice is to make an expansion in terms of Bessel functions[1,2,3]. For calculational simplicity in our case we have chosen rather an expansion in terms of Legendre polynomials whichis also a solution to Laplace's equation[4]. In the case of rotational symmetry ($B_\varphi = 0$), the general expression reduces to

$$B_z = \sum_{i=0}^{\infty} (i+.)\, a_{i+1}\, r^{i}\, P_i\,(\cos\theta) \qquad (3)$$

and

$$B_\rho = \Sigma\ a_{i+1}\, r^{i}\ \sin\theta\, \frac{d}{d\cos\theta} P\ (\cos\theta) \qquad (4)$$

where r is the distance between the point and the origin and θ is the angle between r and the z-axis. The same parameters, a_i, enter into the expressions for B_z and B_ρ because the formulas are derived from a single scalar potential.

The parametrization of the field will be discussed separately for each com- pensation because the procedures were slightly different for each case. This was because of the increasing inhomogeniety which can be seen in Figures 9 through 14.

For the most uniform field (0% compensation), a simultaneous fit was made over the entire measured volume to both B_z and B_ρ values by minimizing the expression

$$\chi^2 = \frac{\Sigma\ (B_z(\text{meas}) - B_z(\text{calc}))^2}{\sigma_z^2} + \frac{\Sigma\ (B_\rho(\text{meas}) - B_\rho(\text{calc}))^2}{\sigma_\rho^2} \qquad (5)$$

This two-dimensional fit takes advantage of all the data and gives a result which is consistent with Maxwell's equations.

Several criteria were used to determine the most suitable number of parameters. As an upper limit the number of parameters should be less than two times the square root of the number of data points to avoid the Runge phenomena. However the r.m.s. difference between the meausred values and the calculated values should be less than the measurement uncertainties. Lastly there is little reason to ncrease the number of parameters beyond the point that the ratio of χ^2 to the number of degrees of freedom becomes constant.

Using this procedure it was possible to obtain a resonable fit with ten parameters. A fit with χ^2/DF much smaller than normally required was also made. This latter fit was used for the second parametrization discussed in the next paragraph in order to minimize the effect of making a least- -squares fit to a least-squares fit. The r.m.s. residuals between the field

calculated using a thirty-one parameter fit (χ^2/DF = 0.098) and the measured field are given in Table 2. A program which gives both field components as a function of position is available. Though the result is satisfactory, the relatively large number of parameters and the time required for evaluating the Legendre polynomial series make this procedure unsatisfactory for use in a track reconstruction program. A technique which is sometimes used to overcome this difficulty is to construct an adequate grid of field values which are stored as a look-up table.

A different approach was used by changing to a one-dimensional fit to a polynomial in z for each of the thirty-six layers in the ARGUS drift chambers. This second parametrization gave a different set of parameters for each layer, but only six or seven parameters at most for each layer. This reduces the computational time to an acceptable level. This second fit was made to the field calculated from the Legendre polynomial series for two reasons : the first parametrization took advantage of Maxwell's equation and, to some extent, corrected the data; furthermore these results can be extended into regions where measurements were not possible, such as the vertex region.

This procedure will obviously give discontinuities between layers, but in practice this has turned out to be acceptable. The results of this fitting procedure and the discontinuity checks are given in Table 2.

For the case of fifty percent compensation the increased inhomogeneity of the field made it desirable to break the field into several regions for the fit to the Legendre polynomial series. Again the fit was made to the B_z and B_ρ data simultaneously. A second parametrization was made as before, resulting in about five parameters for each drift chamber layer and the residuals as shown in Table 2. For the fifty percent case in regions of high field gradient near the compensation coils, a set of cubic spline functions have been provided.

For the most inhomogeneous case, (100% compensation) the Legendre fit was made in one dimension layer by layer, rather than in two dimensions. The polynomial fit was then made exactly as in the case of fifty percent compensation. Again the number of parameters was approximately five for each layer. The results are shown in Table 2. In all of the fitting procedures for each compensation the ratio of χ^2 to the number of degrees of freedom has been much less than unity.

IX. Other Regions

In the vertex region no measurements were taken except on the z axis itself. An extrapolation of the Legendre fit to the z axis gives good agreement as shown in Table 3. A second parametrization was done in layers separated by one cm. The r.m.s. residuals between the Legendre fit and the polynomial fit were between two and five Gauss for all.

In the shower counter region the field was determined using the NUTCRACKER field calculation program from SLAC. The precision is estimated to be approximately 1% in this region.

Inside the compensation coils the results of the NUTCRACKER program were used to establish a grid of field values which was stored and interpolated in two dimensions.

In the case of the shower counter and compensation coil regions the absolute value of the results of the NUTCRACKER program were not used. The results of the program were adjusted so as to match the parametrized field at the boundries of these regions.

Acknowledgements

We would like to thank F. Wittgenstein and the members of the BEBC field mapping system group from CERN for their help in the design and carrying out of the measurements. We gratefully acknowledge the help of H. Albrecht, M. Boileau, H. Schröder and F. Wittgenstein for their part in making the measurements. For suggestions concerning the parametrization we are indebted to H. Albrecht, P. Böckmann, D. Coppage, H. Gennow, P.M. Patel, A. Philipp and H. Schröder. We thank the DESY directorate for their hospitality and support. We want to particularly thank W. Schmidt-Parzefall for his support and encouragement. This work was supported in part by the U.S. Department of Energy Contract DE-AS09-80ER 10690 and by the Department of Elementary Particle Physics, Institute of Physics, University of Lund, Sweden.

TABLE 1

Tests of Symmetry

Compensation	ϕ Symmetry Test		Reflection in mid plane (z=0)		Measurement Uncertainty	
percent	I	II	III	IV	V	VI
	$\frac{B_z - \langle B_z \rangle}{\langle B_z \rangle} \times 100$ rms	$B_z - \langle B_z \rangle$ rms	$\frac{B_z(+z) - B_z(-z)}{\langle B_z(-z) \rangle} \times 100$	$B_z(+z) - B_z(-z)$	σ_z	σ_ρ
	percent	Gauss	percent	Gauss	Gauss	Gauss
0	0.063	4.3	0.063	7.4	14	35
50	0.067	4.6	0.067	9.5	18	44
100	0.075	5.3	0.078	9.5	19	49

REFERENCES

1) J.D. Jackson "Classical Electrodynamics", Wiley, NY (1975) p.108

2) P. Granet and A.C. Melissinos, Cornell report CBX-80-53, Sept. 1980
UR-766, Coo-3065-286

3) R. Frühwirth, Computer Physics Communications 22(1981) 223-229

4) H.M. Fischer and N. Wermes, DESY Internal Rep. F12-80-01

TABLE 3

Extrapolation of Legendre fit to $z=0$, $\rho=0$

Compensation	Data (Gauss)	Extrapolation (Gauss)	Difference (Gauss)
0 %	- 7577	- 7577	0
50 %	- 7514	- 7520	6
100 %	- 7449	- 7456	7

Table 2

Results of Least-Squares Fitting Procedures

Compensation percent		Using Legendre Polynomials $\langle B(\text{fit})-B(\text{data})\rangle_{rms}$ (Gauss)	Using Polynomials in z $\langle B(\text{Legendre})-B(\text{po})\rangle_{rms}$	$\langle B(\text{po})-B(\text{data})\rangle_{rms}$	Discontinuity $\langle B(\text{layer}) - B(\text{layer+1})\rangle_{rms}$
0	B_z	4.9	2.8	6.6	10
	B_ρ	9.8	3.0	11	7
50	B_z	13 in sensitive d.c. area 56 outside	4	21	16
	B_ρ	15 in sensitive d.c. area 65 outside	5	22	4
100	B_z	7	3	9	9
	B_ρ	15	5	16	9

FIGURE CAPTIONS

Fig. 1. The ARGUS Detector

Fig. 2. ARGUS Coordinate System

Fig. 3. Compensation Coil Connections

Fig. 4. Mechanical Mounting of Probes
a) Overall view, b) schematic drawing of probe support arms, c) end view of one support

Fig. 5. Measuring Grid

Fig. 6. Magnetization Measurement

Fig. 7. Residuals between B_φ (measured) and B_φ (calculated)

Fig. 8. B_ρ as a function of z

Fig. 9. Measured B_z field at 0% compensation

Fig. 10. Measured B_z field at 50% compensation

Fig. 11. Measured B_z field at 100% compensation

Fig. 12. Measured B_ρ field at 0% compensation. Corrected for probe misaligrment

Fig. 13. Measured B_ρ field at 50% compensation. Corrected for probe misaligrment.

Fig. 14. Measured B_ρ field at 100% compensation. Corrected for probe misaligrment.

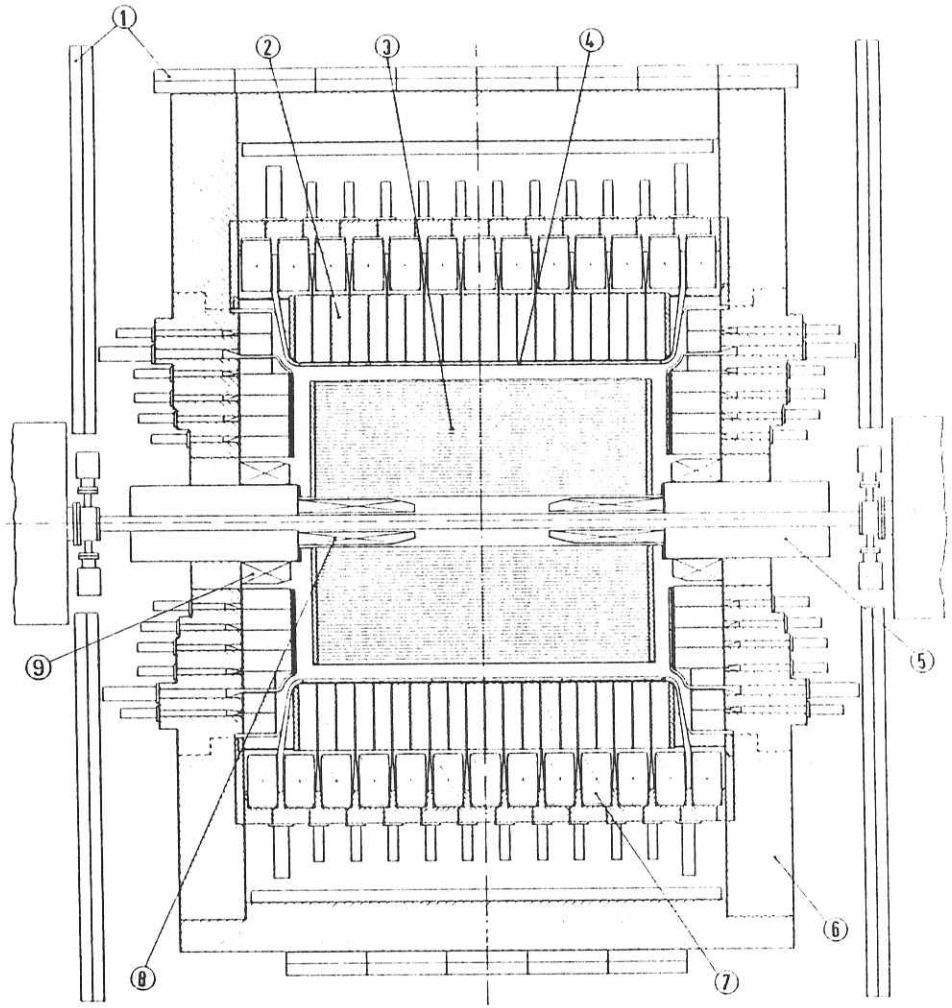

1. Muon chambers
2. Shower counters
3. Drift chamber
4. Time of flight counters
5. Mini beta quadrupole
6. Iron yoke
7. Solenoid coils
8. Compensation coils (inner)
9. Compensation coils (outer)

Fig. 1

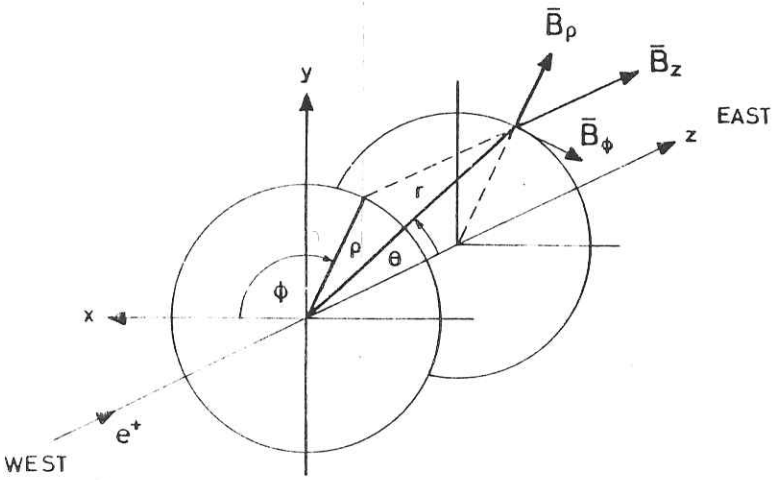
$\bar{B}_\rho$
$\bar{B}_z$
$\bar{B}_\phi$
y
EAST
z
r
ρ
θ
ϕ
x
e+
WEST

Fig. 2

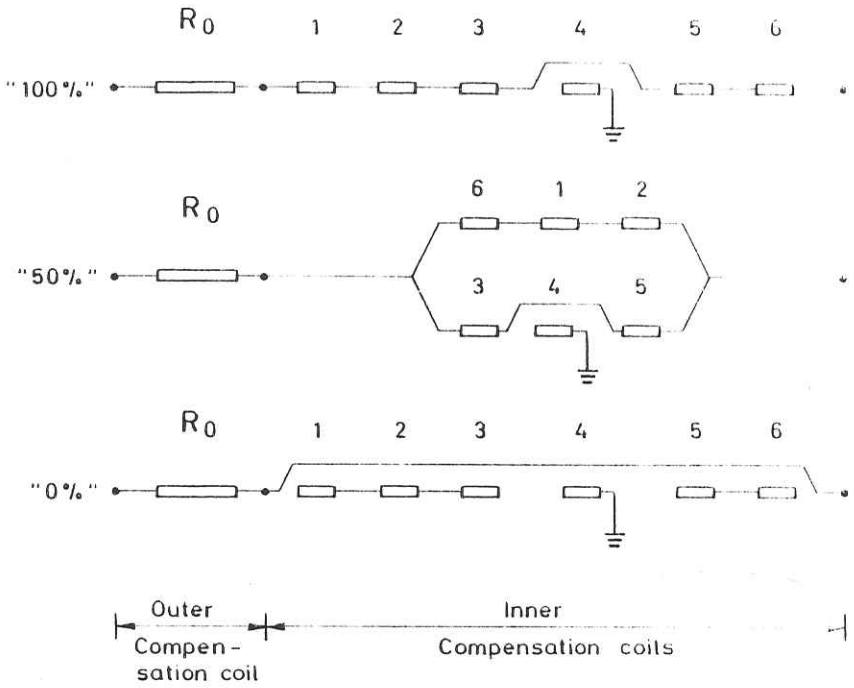
R0
1
2
3
4
5
6
"100%"
R0
6
1
2
3
4
5
"50%"
R0
1
2
3
4
5
6
"0%"
Outer
Compen-
sation coil
Inner
Compensation coils

Fig. 3

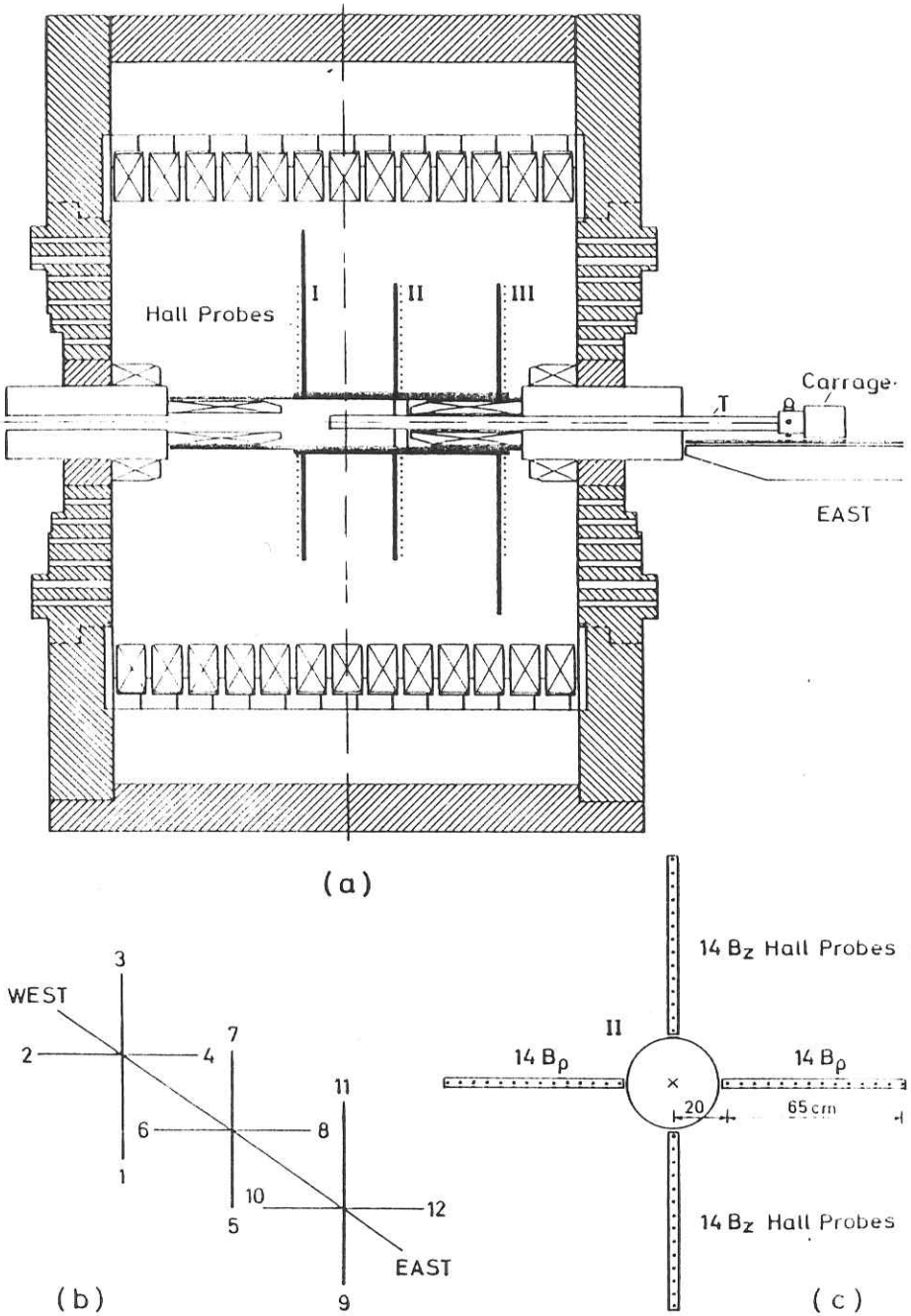
Hall Probes
I
II
III
Carrage
T
EAST
(a)
WEST
3
2
4
7
6
8
11
1
10
12
5
9
EAST
(b)
14 Bz Hall Probes
II
14 Bρ
14 Bρ
20
65 cm
14 Bz Hall Probes
(c)

Fig. 4

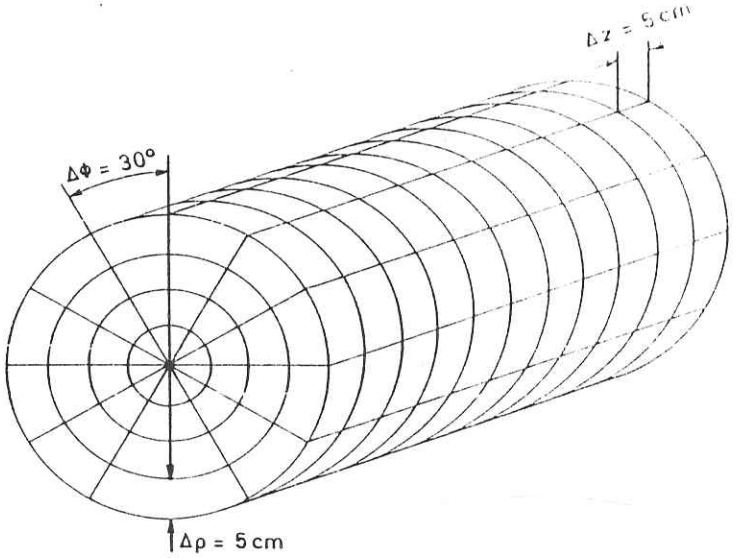
Δz = 5 cm
Δφ = 30°
Δρ = 5 cm

Fig. 5

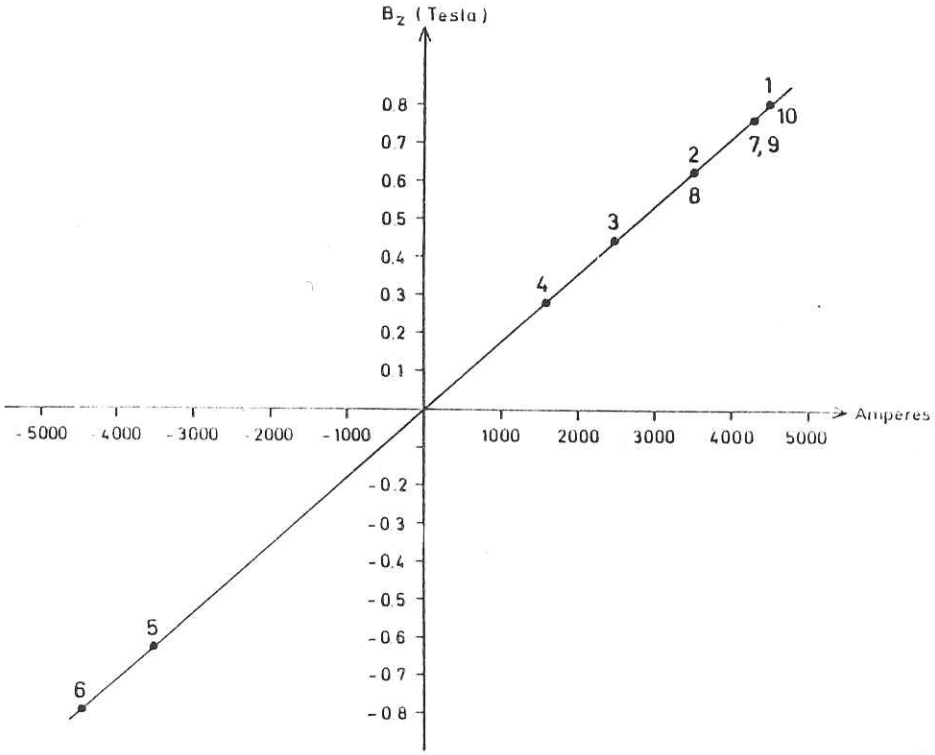
B_z (Tesla)
0.8
0.7
0.6
0.5
0.4
0.3
0.2
0.1
-0.2
-0.3
-0.4
-0.5
-0.6
-0.7
-0.8
-5000
-4000
-3000
-2000
-1000
1000
2000
3000
4000
5000
Amperes
1
10
7,9
2
8
3
4
5
6

Fig. 6

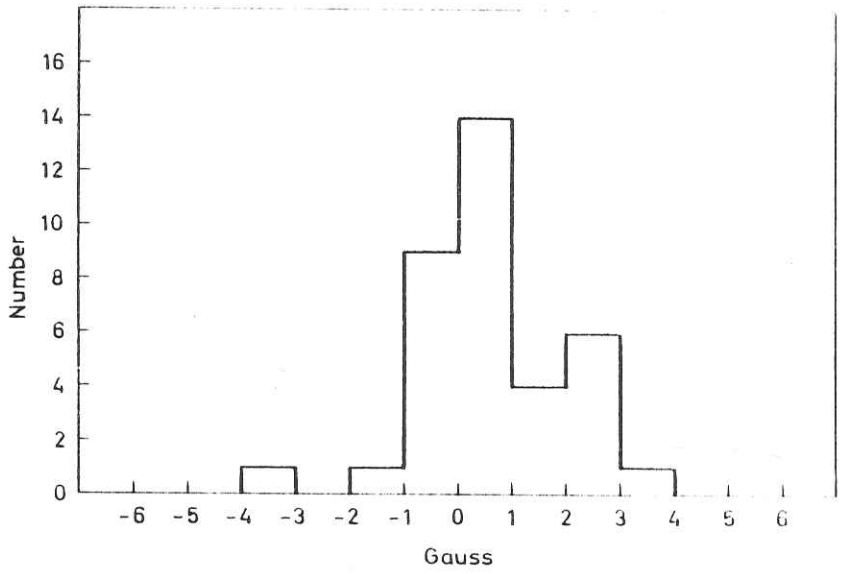
Number
16
14
12
10
8
6
4
2
0
-6
-5
-4
-3
-2
-1
0
1
2
3
4
5
6
Gauss

Fig. 7

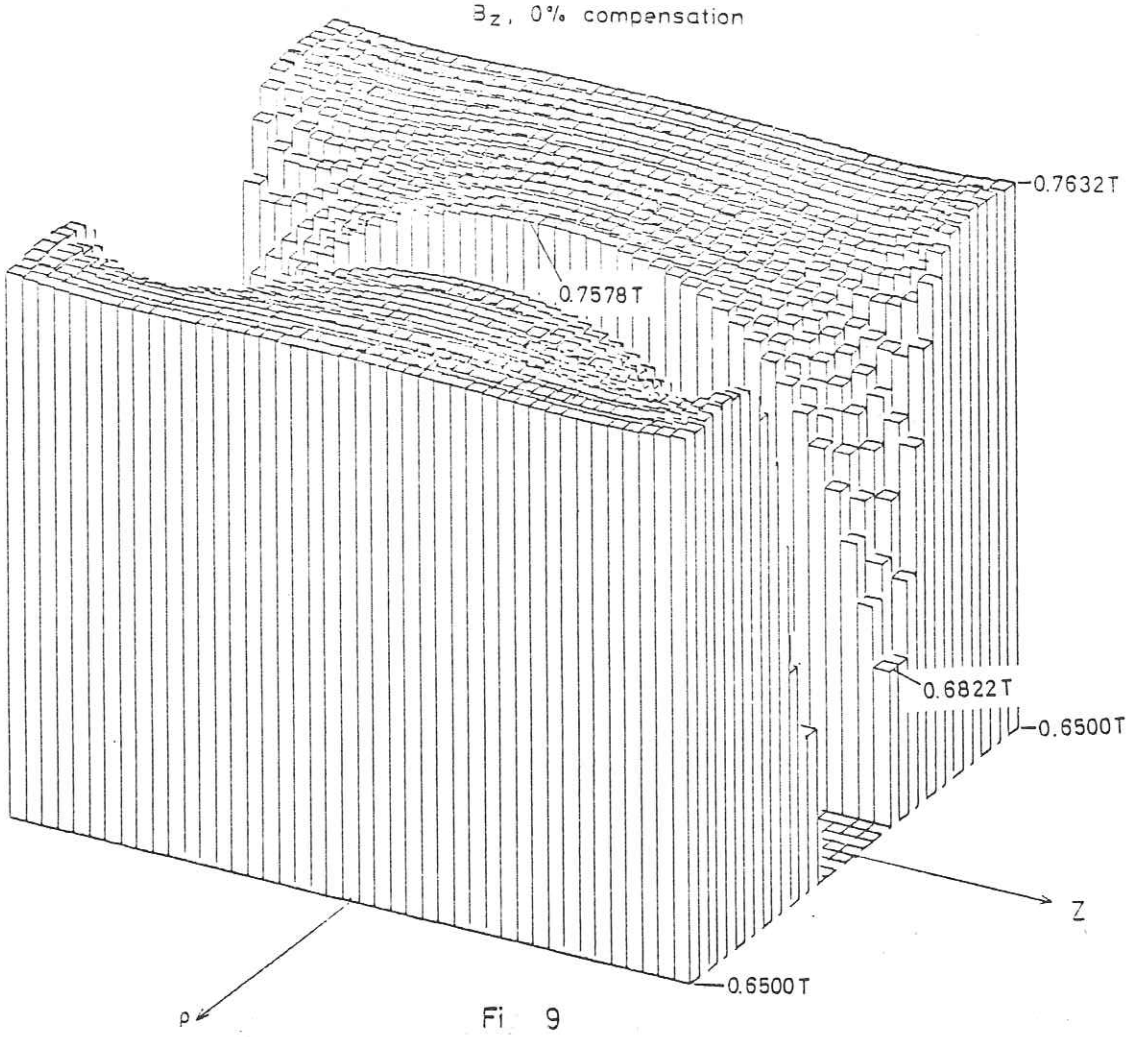
B_z, 0% compensation
0.7632T
0.7578T
0.6822T
0.6500T
0.6500T
Z
ρ

Fi 9

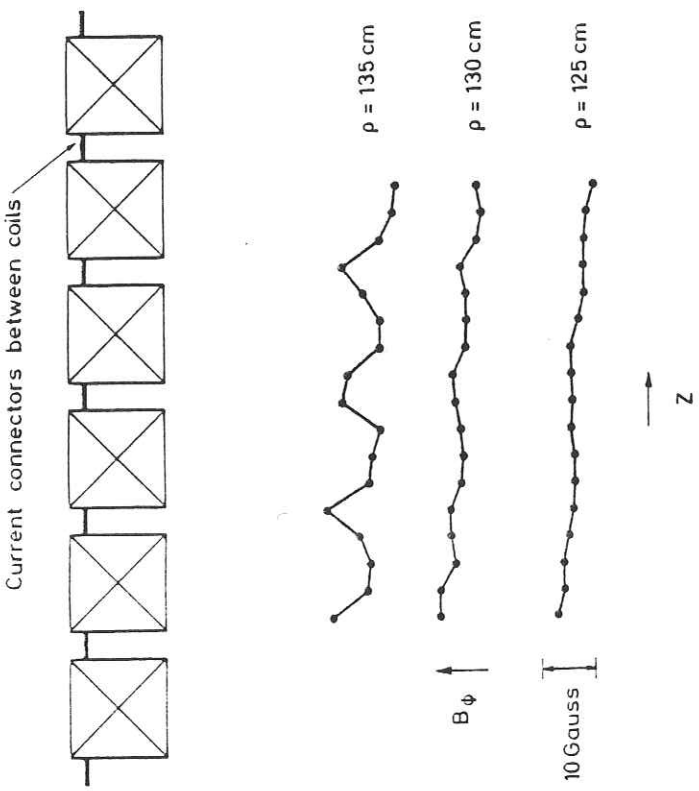
Current connectors between coils
ρ = 135 cm
ρ = 130 cm
ρ = 125 cm
B_ϕ
10 Gauss
z

Fig. 8

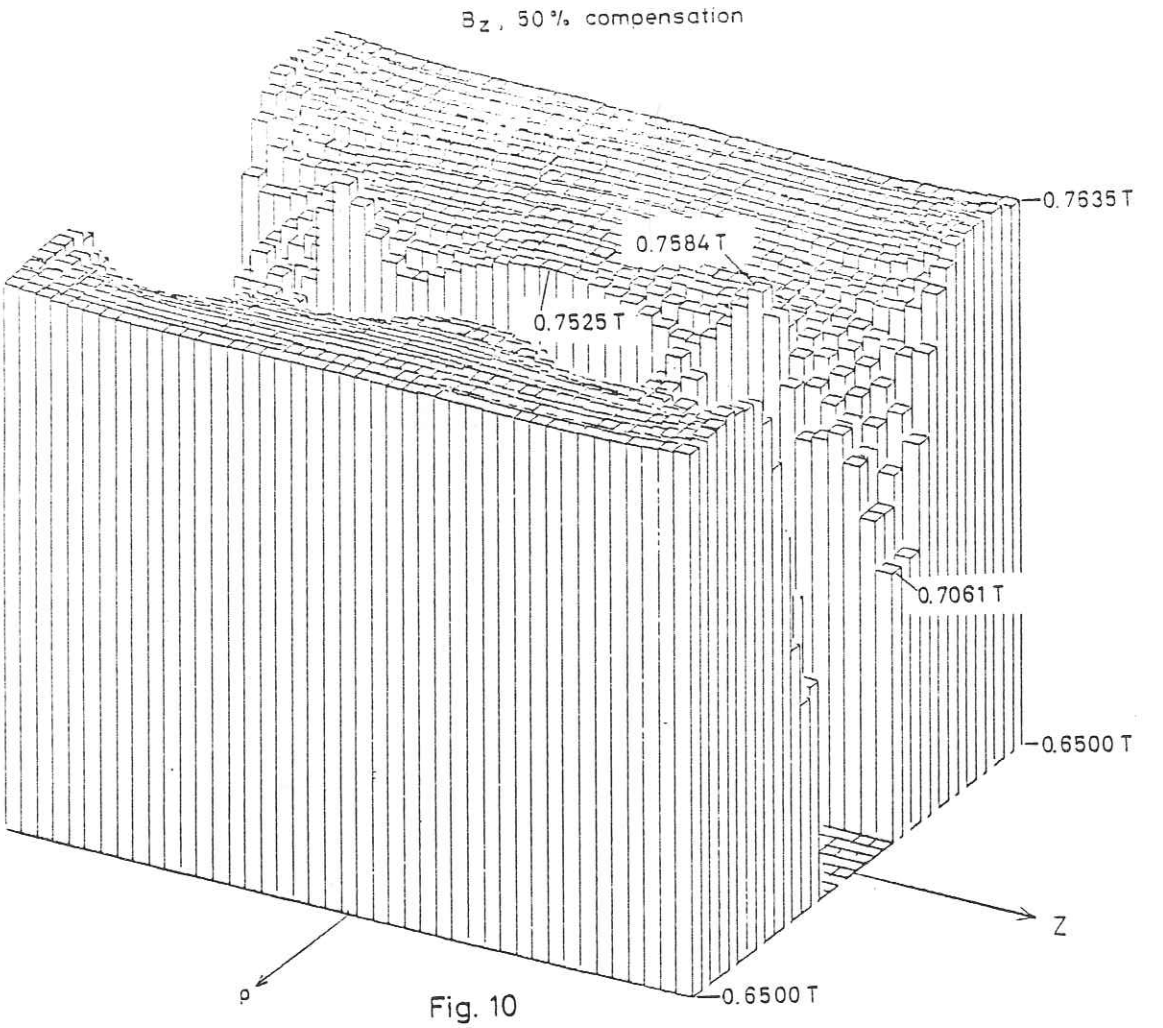
B_z , 50 % compensation
0.7635 T
0.7584 T
0.7525 T
0.7061 T
0.6500 T
Z
ρ
0.6500 T

Fig. 10

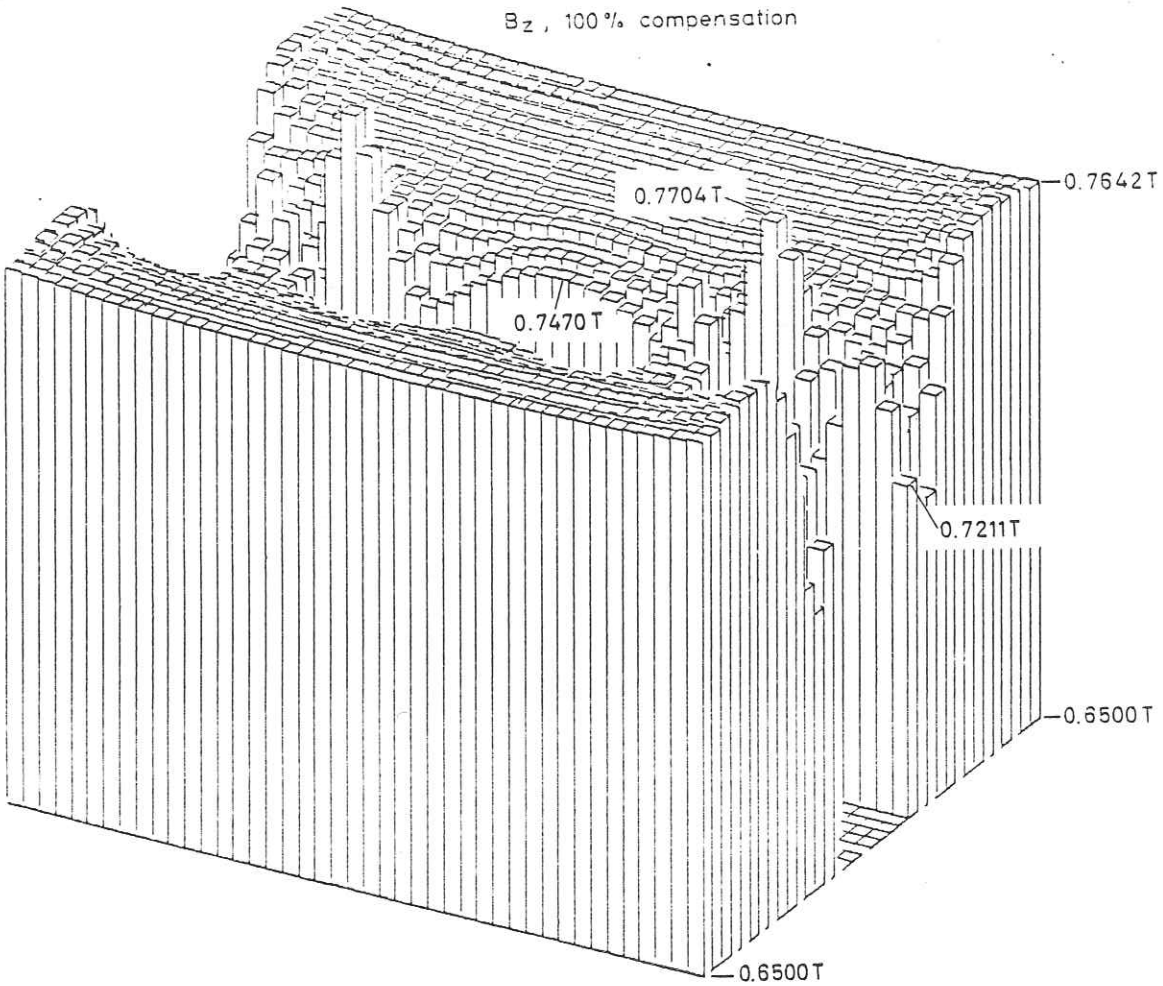
B_z , 100 % compensation
0.7642 T
0.7704 T
0.7470 T
0.7211 T
0.6500 T
0.6500 T

Fig. 11

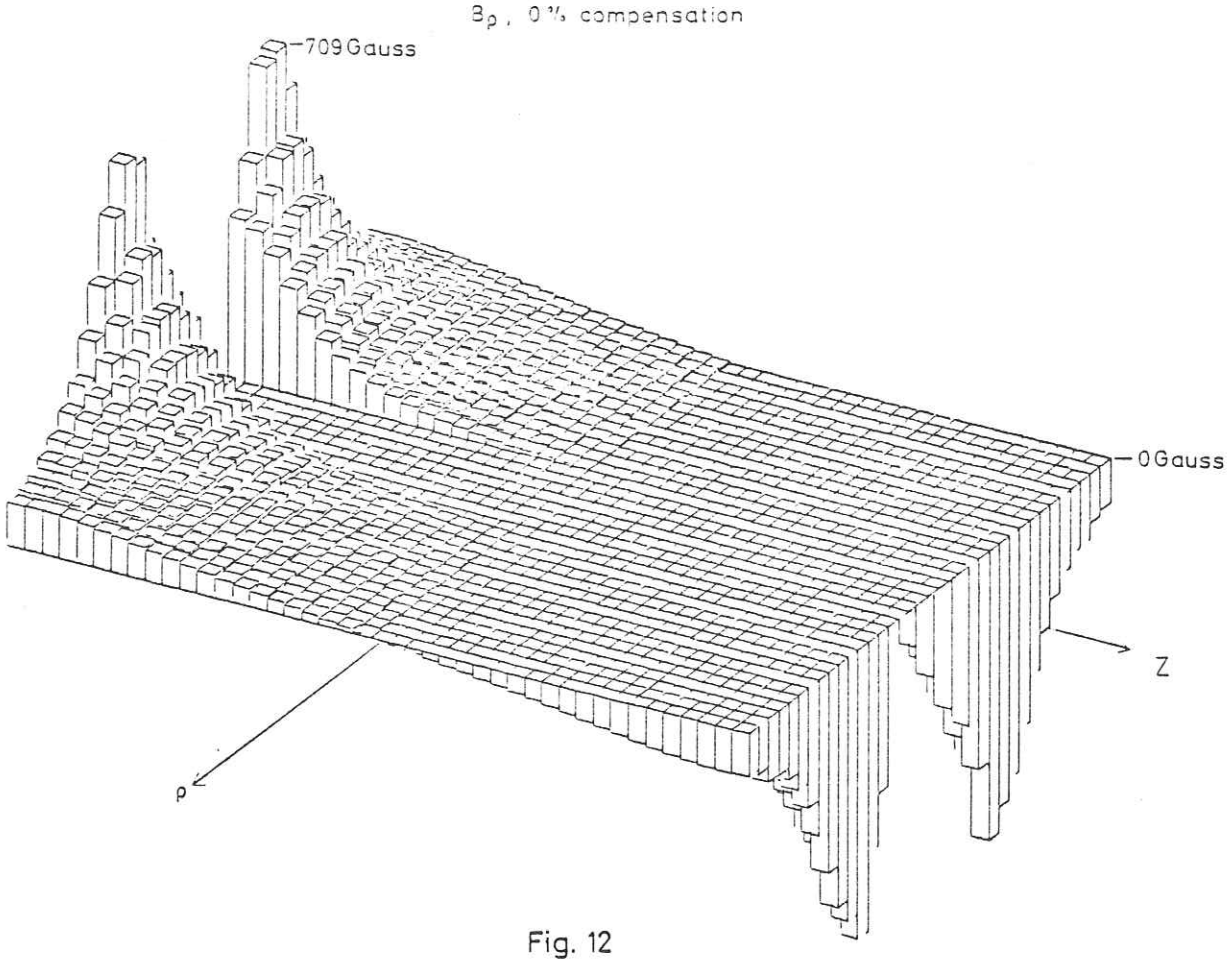
B_ρ , 0 % compensation
709 Gauss
0 Gauss
Z
ρ

Fig. 12

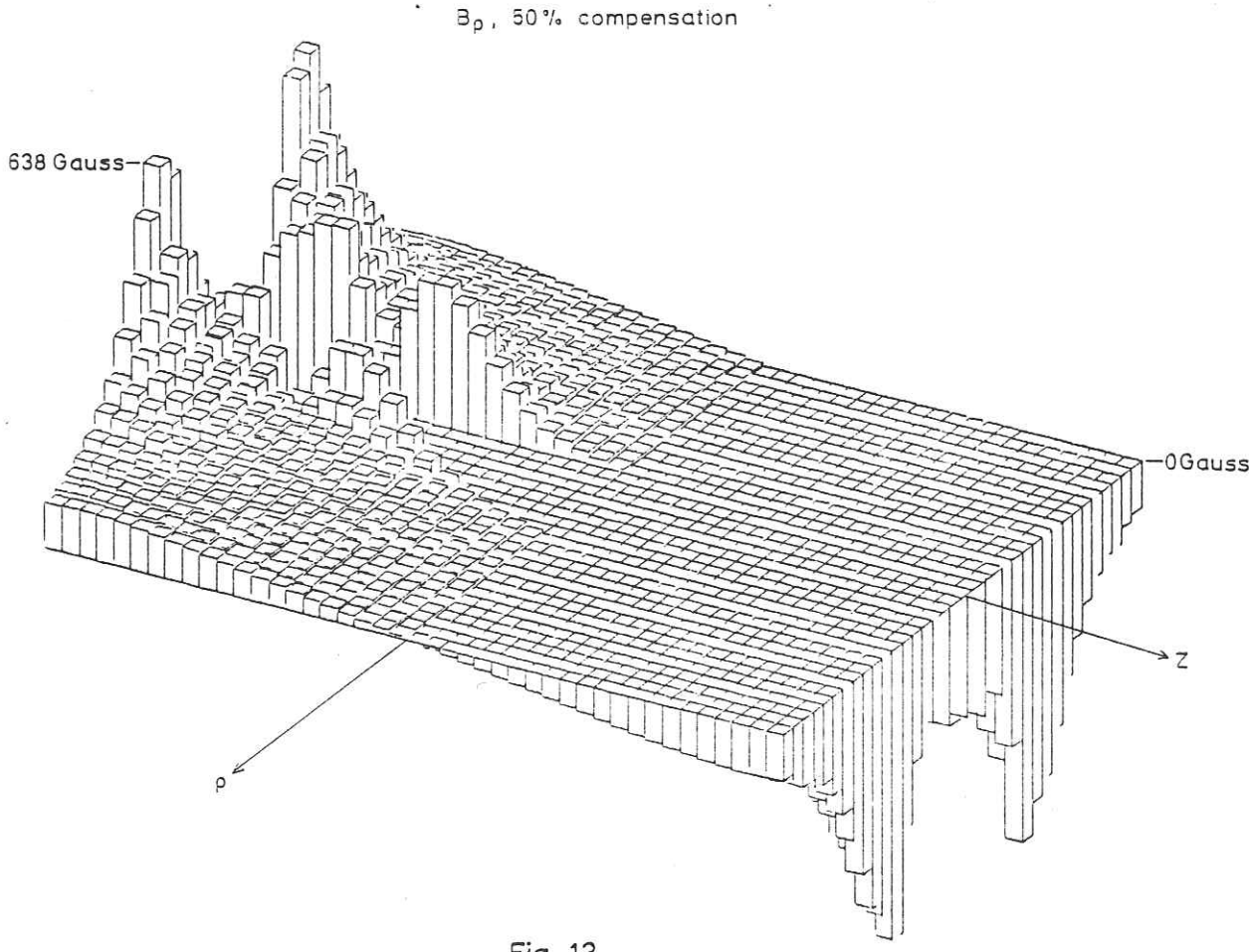
B_ρ , 50 % compensation
638 Gauss
0 Gauss
Z
ρ

Fig. 13

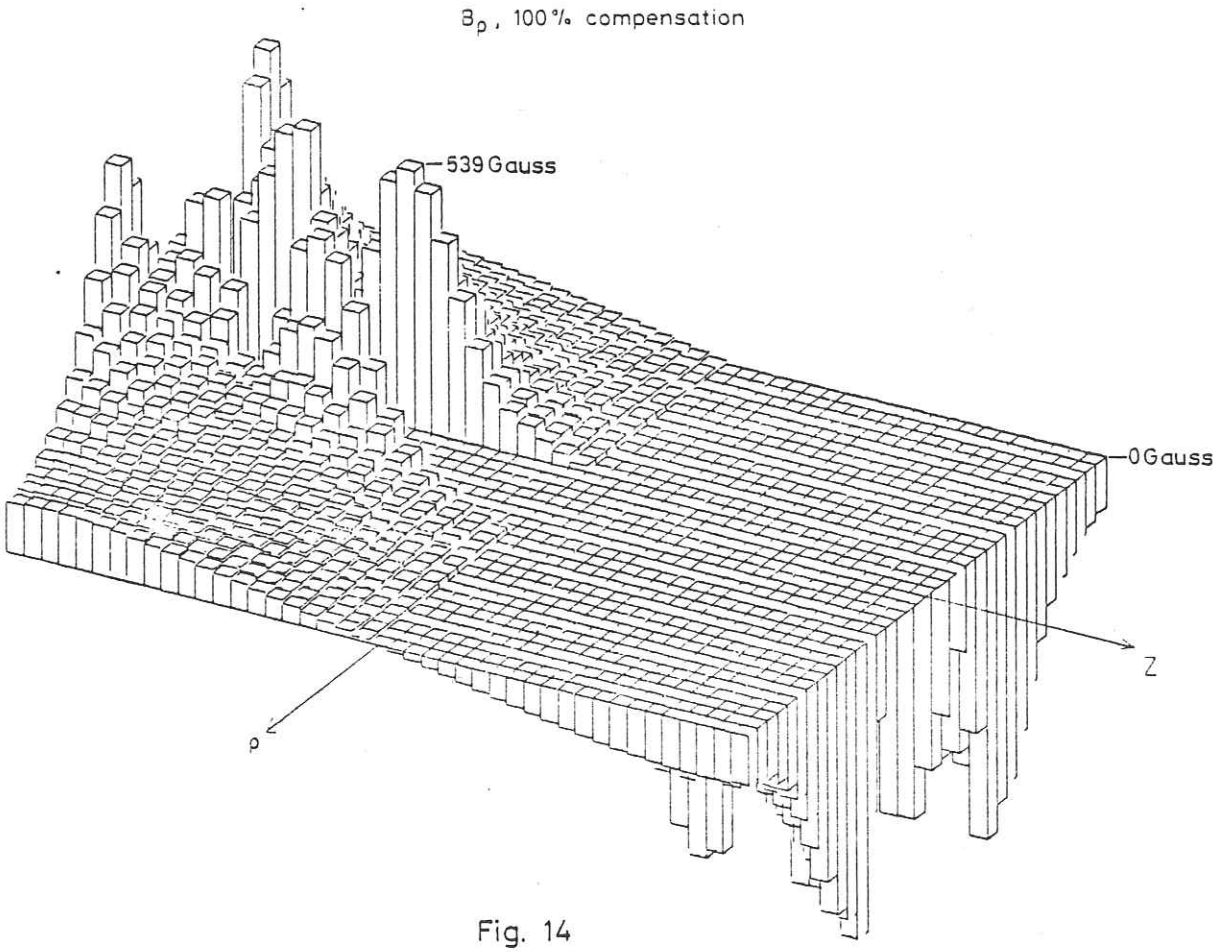

Fig. 14